Exp Fluids (2012) 52:519–527
DOI 10.1007/s00348-011-1240-x

RESEARCH ARTICLE

Fourier transform profilometry for water waves: how to achieve clean water attenuation with diffusive reflection at the water surface?

A. Przadka · B. Cabane · V. Pagneux · A. Maurel · P. Petitjeans

Received: 2 September 2011 / Revised: 6 November 2011 / Accepted: 23 November 2011 / Published online: 3 December 2011

Abstract We present a study of the damping of capillary-gravity waves in water containing pigments. The practical interest comes from a recent profilometry technique (FTP for Fourier Transform Profilometry) using fringe projection onto the liquid-free surface. This experimental technique requires diffusive reflection of light on the liquid surface, which is usually achieved by adding white pigments. It is shown that the use of most paint pigments causes a large enhancement of the damping of the waves. Indeed, these paints contain surfactants which are easily adsorbed at the air–water interface. The resulting surface film changes the attenuation properties because of the resonance-type damping between capillary-gravity waves and Marangoni waves. We study the physicochemical properties of coloring pigments, showing that particles of the anatase (TiO_2) pigment make the water surface light diffusive while avoiding any surface film effects. The use of the chosen particles allows to perform space-time resolved FTP measurements on capillary-gravity waves, in a liquid with the damping properties of pure water.

A. Przadka · B. Cabane · P. Petitjeans (✉)
Laboratoire de Physique et Mécanique des Milieux Hétérogènes (PMMH), UMR CNRS 7636–ESPCI–UPMC Univ. Paris 6–UPD Univ. Paris 7, 10 rue Vauquelin, 75005 Paris, France
e-mail: phil@pmmh.espci.fr

V. Pagneux
Laboratoire d'Acoustique de l'Université du Maine, UMR CNRS 6613, Avenue Olivier Messiaen, 72085 Le Mans, France

A. Maurel
Institut Langevin LOA, UMR CNRS 7587–ESPCI–UPD Univ. Paris 7, 10 rue Vauquelin, 75005 Paris, France

1 Introduction

Free surface waves are an important subject in fluid dynamics due to their practical applications in the industry (such as naval architecture, coastal and ocean engineering) and also due to the wealth of physical phenomena that they display. Most experimental studies on liquid surface deformation have used qualitative direct visualizations of the 2D surface or quantitative one-point temporal measurements. Recently, our group has proposed a full space-time resolved measurement of the surface elevation, using a technique called Fourier transform profilometry (FTP). This technique was first developed by Takeda et al. (1982), Takeda (1983) for solid surfaces. We have improved and implemented it for liquid surfaces (for details and bibliography see Maurel et al. 2009; Cobelli et al. 2009; Gorthi 2010). Typical examples of measured wave fields are shown in the Fig. 1. In the first example, a plane wave propagates with defined frequency ω over a nonuniform bottom producing wave scattering. Owing to the temporal resolution, the total measured displacement field $h(x, y, t)$ can be easily expanded in $h(x, y, t) = \sum_n Re[h_n(x, y)e^{in}\omega t]$ to extract the complex field h_1 that is later analyzed. The second example is of particular interest with respect to the purpose of this paper.[1] In the case of wave turbulence experiments, the water wave field results from the nonlinear interactions of random waves. The theoretical predictions in weak turbulence theory are done in the Fourier (k, ω)-space, and this space becomes accessible

[1] The effect of monomolecular surface film, that we want to avoid, has been studied in Alpers (1989), where the authors show that the power law of the energy spectra in water wave turbulence can be modified by the presence of a surface film.

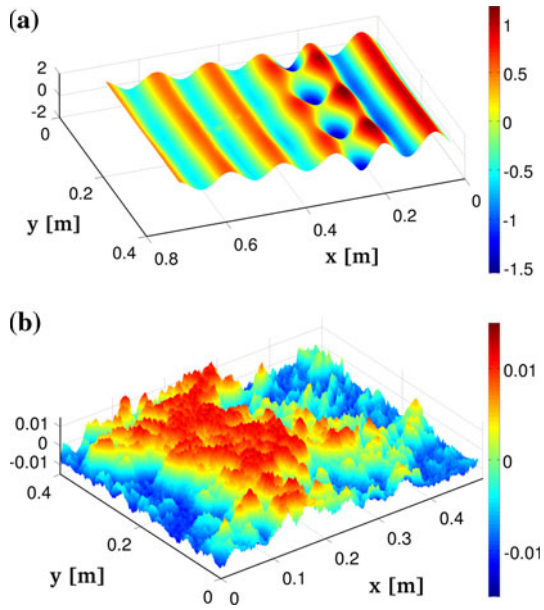

Fig. 1 Example of FTP measurements in water wave experiments: **a** real part of the wave field $h_1(x,y)$ in experiments of wave propagating over a nonuniform *bottom*. The complex field h_1 is obtained by extracting the Fourier component of the total measured field. *Colorbar* is in mm. **b** Instantaneously measured velocity field in experiments of wave turbulence. The measure of $h(x, y, t)$ gives access to the Fourier (k, ω)-space for comparison with theoretical predictions. *Colorbar* is in m/s

experimentally thanks to our full space-time resolved method.

Since the FTP method uses the deformation of fringes projected onto the free surface, this surface must scatter light. It is not possible with pure water, which is transparent and has a very low surface reflectance. Previously, light diffusivity was achieved by diluting white paint in water. This produced a substantial increase in the scattering from water (in the reflectance of the water surface). However, it was also found that the attenuation of surface waves was dramatically enhanced compared to that of pure water. This spurious attenuation is particularly harmfull when studying wave phenomena. It was soon found that it is caused by the presence of a film at the surface of water. Indeed, water is a liquid that has an unusually high cohesion and, therefore, a very high surface tension. Consequently, many species adsorb to the water–air interface, either from the water side (dissolved species) or from the atmosphere (airborne molecules or particles). These species quickly create a film at the water surface and this film may strongly change the attenuation properties of surface waves: this phenomenon is well known since the observations of the "calming effect of oil on water" by Benjamin Franklin in the eighteenth century (Franklin 1774; Behroozi et al. 2007). Since then, the attenuation due to the excitation of surface film vibrations by water waves has been studied in details by several authors (Alpers 1989; Levich 1962; Miles 1967; Lucassen 1968, 1982; Lange 1984).

We have found a way to make the water light diffusive while keeping its low attenuation property. The solution to this problem required investigation into the surface chemistry of the pigments. It also involved the use of rigorous methods to ensure good pigments dispersion without release of any surface active molecules in water (not even traces!).

This paper is organized as follows: Section 2 is dedicated to the choice and characterization of nonsurface active aqueous dispersions that can make water light diffusive while avoiding the formation of a surface film. To verify the absence of a surface film, the measurement of the surface tension of the dilute aqueous dispersions was performed. In Sect. 3, we present FTP measurements of the water wave attenuation, comparing water colored by plain paint to the dispersion of nonsurface active particles. It is also confirmed that the chosen particles allow us to restore the attenuation of pure water. Incidentally, it is shown that the enhancement of attenuation by plain paint is associated with a resonance of the film surface, in agreement with the theory (Alpers 1989; Lucassen 1968, 1982).

2 Nonsurface active dispersions

The desired characteristics of the pigment particles are threefold: (a) they must provide a high reflectance of the water surface; (b) they must be well dispersed in water; (c) they must not release any surface active molecules or ions that would form a film at the surface of water. To a large extent, these constraints are in conflict with each other and this is what makes the choice of the pigments difficult.

In order to meet condition (a), the classical choice is to use titania (TiO_2) particles. Indeed, titania has a very high refractive index ($n = 2.7$), nearly the highest among minerals. With this high refractive index, the optimum size of the titania particles is about 300 nm, which is the average size of commercially available TiO_2 pigments. Particles of this size are strongly agitated by Brownian motions and sediment quite slowly, unless they aggregate.

Condition (b) is not easily met for pure titania particles, for two reasons. Firstly, titania surfaces are ionized in water according to the classical reaction schemes:

$$\begin{aligned} &\mathrm{Ti-OH + OH^- \leftrightarrow TiO^- + HOH},\\ &\mathrm{Ti-OH + OH_3^+ \leftrightarrow TiOH_2^+ + HOH} \end{aligned} \tag{1}$$

If one of these reactions prevails, the surface acquires a net electrical charge and the corresponding electrical potential attracts a double layer of counterions in the

vicinity of the surface. When particles approach each other, the overlap of the diffuse layers of counterions gives rise to the classical DLVO repulsions, which keep the surfaces apart and prevent particle aggregation (Evans 1994; Israelachvili 1991; Hunter 1981). However, for titania, their reactions are balanced at pH = 6, which means that the surface has an isoelectric point at this pH. Consequently, the titania surfaces do not retain any electrical double layers of counterions, and when particles approach each other, the classical DLVO repulsive forces are absent. This is true for both common crystalline forms of titania, that is, anatase and rutile.

In order to prevent the aggregation of titania particles in water, the particles' surfaces are usually covered either with a layer of another oxide (e.g., silica or alumina) or with adsorbed polyelectrolytes, such as polyacrylates. These changes shift the zeta potential curve and the location of the isoelectric point on the pH scale. Figure 2 shows the results of measurements of the electrophoretic mobility of various titania dispersions, here expressed in terms of the zeta potential, which is the electrical potential at the shear plane near the particle surface. The titania pigments provided by Kronos International, Inc. have been applied in all our dispersions.

These values of the zeta potential make it possible to predict the aggregation behavior of the various titania dispersions. Indeed, it is known from DLVO theory that zeta potentials above 40 mV provide strong electrical double layer repulsions and, therefore, predict adequate colloidal stability. Conversely, zeta potentials below 30 mV do not provide sufficiently strong electrical double layer repulsions, especially for the case of particles that have strong Van der Waals attractions as is the case for titania particles.

According to the results shown in Fig. 2, the rutile TiO_2 coated with alumina would only be acceptable at pH $\leq$ 3, which is too acidic to be handled in a large water tank with delicate electrical and optical equipment. Similarly, the rutile TiO_2 coated with alumina and silica would not aggregate in a solution with pH $\geq$ 9, but this is not acceptable in a laboratory with standard instrumentation.

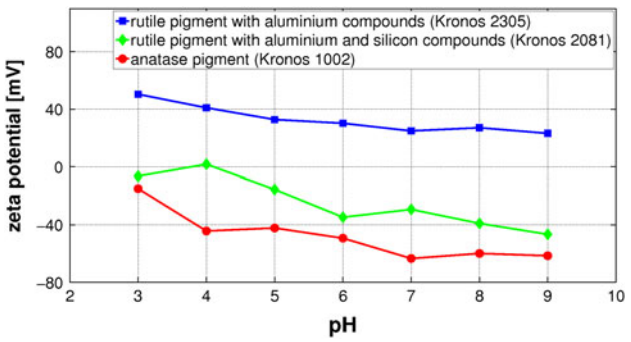

Fig. 2 Zeta potential as a function of pH

Nowadays, many titania dispersions have gained a surface charge and a high zeta potential through the adsorption of polycarboxylates, e.g., sodium polyacrylate or sodium citrate. However, the molecules are only physically bound to the titania surfaces through ionic interactions with the surface sites. A fraction of these molecules is always released in water, either because the adsorption forces are not infinitely strong or because the manufacturer has added an amount of the molecules that exceeds the saturation level of the surface (most likely). It is then in conflict with condition (c), because these excess molecules are surface active and, therefore, spontaneously adsorb and form a film at the free water surface. Indeed, we have found that all water-dispersible pigments that are made of particles with "dispersants" adsorbed on their surfaces fail to pass condition (c), as defined by the criteria presented below.

Figure 2 shows that the anatase pigment is for us the best choice since it has a zeta potential $Z_p < -40$ mV in all aqueous solutions with pH > 4. It is then possible to use pure water to disperse these particles. The water used in our experiment is purified. Its resistivity is greater than 16 MΩ cm, and its surface tension is 71 mN/m.

It is then necessary to verify that condition (c) is met with the chosen pigment. For this purpose, some experimental criteria and procedures must be defined. A criterion for the presence or absence of a film at the water surface is the value of the surface tension. If p_{film} is the film pressure, γ the measured surface tension and γ_0 the surface tension of pure water, then

$$\gamma = \gamma_0 - p_{\text{film}}$$

Typical values of p_{film} are 20 mN/m for water surfaces exposed to open air and 40 mN/m for water containing dissolved surface active molecules. Thus, a practical criterion for assessing the absence of adsorbed films at the water surface is that the measured surface tension should be within 5 mN/m of that of pure water. As noted previously, the absence of any surface film is not easily achieved with water containing dispersed pigments, as most commercially available pigments release surface active species in water. In contrast, aqueous dispersions made with the anatase pigment had surface tensions above 70 mN/m. This surface tension decreased very slowly with time because of adsorption of surface active species that have migrated from the air or other parts of the equipment (Prisle et al. 2008). A brief aspiration of the surface layer brought it back to its initial value.

For FTP experiments, it is useful to characterize the reflectance of the water surface (condition (a)) in terms of the contrast. The contrast is defined as the number of intensity gray levels between the white and black fringes.

The better resolved is the fringe signal recorded by the camera, the better resolution on the measured surface shape. This is because the resolution in the FTP measurements depends on this contrast (for more technical details see Sect. 3.1). This contrast is a combination of the absolute reflectance of the particles, of the characteristics of the projecting device and of the characteristics of the camera. In our studies, we have obtained accurate measurements for at least 50 gray levels between white and black fringes, while the contrast below 20 gray levels was found to be critical.

Figure 3 illustrates the contrast as a function of the concentration of anatase (rutile pigments are given for comparison). For the chosen anatase particles, the contrast of 50 is obtained for a concentration of 2 g/l.

Finally, the particle sedimentation has been analyzed for the chosen anatase pigment. Settling out process causes the light to be diffused not from the surface, but from the lower layer of the dispersion and this induces an error in the measurements. The sedimentation speed v can be calculated by equaling the gravity force and viscous resistance of the water

$$v = \frac{2}{9}\frac{r^2 \Delta\rho g}{\mu}, \qquad (2)$$

where r stands for particle radius, g for the gravity acceleration, and $\Delta\rho = 2.8\,\mathrm{g/cm^3}$ for the density difference between the particles and water, and $\mu = 10^{-3}$ Pa.s for the dynamical viscosity. The measurements of the particles' size for the pH in the electrically stable range showed the particle diameter to be 350 ± 50 nm.

Figure 4 illustrates the effect of the particles' sedimentation on the FTP measurements. The liquid was agitated at the initial time, and then the elevation of the free surface was measured at several times in two cases: I) the liquid was not shaken anymore (it remained at rest) during the whole experiment, and II) the liquid was excited by the wavemaker for a short time between two measurements.

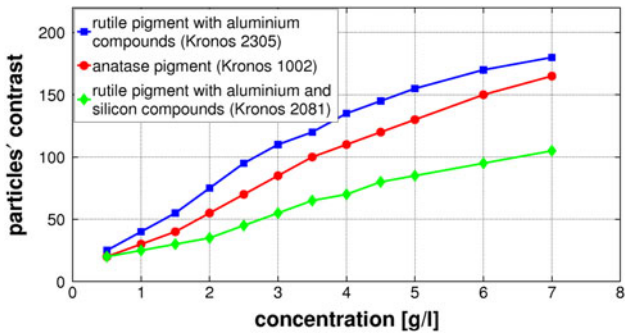

Fig. 3 Contrast as a function of the particles' concentration for anatase pigment and rutile pigments. The camera worked at 8 bits (256 gray levels)

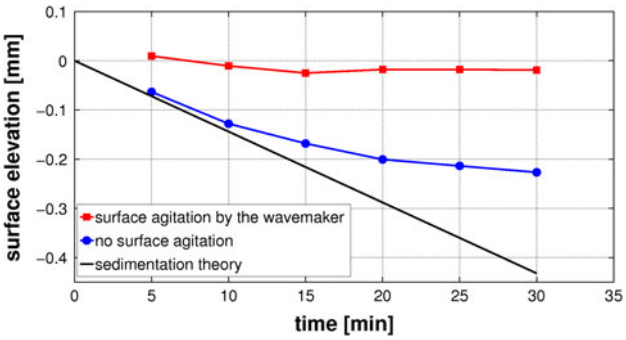

Fig. 4 The apparent surface position, as measured by FTP, as a function of time for two cases: no liquid shaking (*blue curve*), the liquid was excited by waves produced by a wavemaker during a short time between two measurements (*red curve*). *Black curve* shows the theoretical prediction for the sedimentation (Eq. 2, using the mean size of the particles). The dispersion used here is the anatase with a concentration of 4 g/l. The real position of the free surface is at zero (the *errorbar* is 0.02 mm)

In the first case, the free surface position seems to decrease in time which is connected with particles' sedimentation. Initially, sedimentation follows reasonably the theoretical prediction (black curve in the Fig. 4) using Eq. 2 with r the mean size of the particles. Then, the particles seem to sediment slower. It is connected with the existence of smaller particles which settle out slower. In the case II, the free surface position varies around the zero level within the error bar. This means that the motion induced by the wave propagation provides enough mixing to prevent the sedimentation effect.

3 FTP measurement of water wave attenuation

In 1872, Marangoni described the effect of surface tension gradients. He found that they alter the tangential stresses balance on the surface: while the wave passes, it locally expands (at the wave back) and compresses (at the wave front) the surfactant monolayer causing locally higher and lower surface tension areas due to the local differences in surfactant density. In 1968, Lucassen proved the existence of longitudinal waves on the surface film accompanying the capillary-gravity waves. These waves are governed by the surface elastic modulus of the film rather than by the surface tension and the gravity. Because of the tangential surface stresses, the kinematic boundary condition on the surface is changed, implying that the linearized Navier–Stokes equation has two different solutions: one describing well-known water waves and another one describing longitudinal waves (often called Marangoni waves).

In the past, the calming effect due to the monomolecular slicks existence has been supposed to affect only the capillary waves. Few years later, Lucassen (1982), Cini et al.

(1987) showed that such a film can induce the resonance-type wave damping between Marangoni and capillary-gravity waves, which results in a large attenuation enhancement also in the short-gravity-wave region. At the same time, the experimental evidence of the higher energy dissipation of the short gravity waves was given by Lange (1984) in the laboratory scale and by Ermakov et al. (1986) in the open sea. The mathematical description of the problem, originally proposed by Alpers (1989), can be found in the "Appendix".

3.1 Experimental details

The presented experiments were performed in the rectangular basin of 160×60 cm^2. The industrial titanium dioxide anatase particles (Kronos 1002) with a concentration 4 g/l were used to color water of 5 cm depth. The surface tension γ was measured before and regularly during experiments by Krüss K100 Tensiometer using the ring method and was equal to 71 ± 1 mN/m for water with titania particles (and 32 ± 1 mN/m for water colored by plain paint). Water temperature was maintained at 17 ± 1°C.

The FTP method implemented by Maurel et al. (2009) and Cobelli et al. (2009) was applied to measure the surface elevation $h(x, y, t)$. In the FTP method, a fringe pattern is projected onto the free surface and observed from a different position by the camera. The surface elevation information is encoded in the fringes deformation in comparison with the original (undeformed) grating image. It is, therefore, the phase shift between the reference and deformed images which contains all information about the deformed surface (see Lagubeau et al. 2010; Cobelli et al. 2009, 2011a, b, for the examples of applications).

A Phantom v9 high-speed camera was used to record the surface of 30×30 cm^2 area with a 560×560 pix^2 and a sampling frequency $f_s = 160$ fps. The horizontal resolution was equal to 0.53 mm, which corresponds to the pixel size. The vertical precision was estimated to 0.1 mm with an error of 0.05 mm. It was found to be sufficient to reconstruct the waves with typical wavelength 3–15 cm and amplitude of few millimeters (to avoid the nonlinear effects).

The experiment consists in recording the transient wave produced by a broadband wavepacket signal (modulated with a blackman window). In the case of water colored by the titania particles, the central frequency of the signal was 8 Hz and the sampling was chosen such that 20 points were recored per period. A single input signal allowed us to treat broad frequency range between 4 and 10 Hz. For water colored by plain paint, the damping is enhanced, so the frequency range around the central frequency with energy above the noise level is reduced. Thus, five different input signals were used with central frequency at 4, 5, 6, 7 and 8 Hz. The images recording finished after capturing 16,000 images (100 s), which was enough for the waves to be totally attenuated.

Since the depth of the water is constant, in the harmonic regime, at pulsation ω, it can be shown that the height perturbation is the solution of the Helmholtz equation:

$$(\triangle + \mathbf{k}^2)H = 0, \tag{3}$$

where $\mathbf{k}$ is linked to the pulsation ω by the linear dispersion relation. It is important to notice that $\mathbf{k}$ has an imaginary part due to the attenuation ($\mathbf{k} = \kappa + \mathrm{i}\beta$, where κ, β are real). In the above equation, $\mathbf{k}$ is the unknown and H stands for the time Fourier transform of the measured transient height $h(x, y, t)$:

$$H(x, y, \omega) = \int_{-\infty}^{\infty} h(x, y, t) \cdot \mathrm{e}^{-\mathrm{i}\omega t} \mathrm{d}t \tag{4}$$

The FTP measurement of the transient h allowed to obtain the H fields for a broad range of frequencies with 0.01 Hz step.

An example of the measured H field is shown in the top of the Fig. 5. Owing to the spatial resolution of the FTP

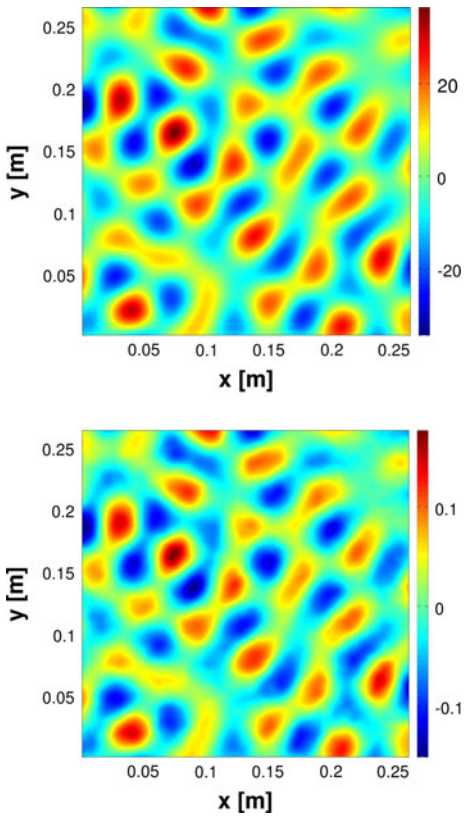

Fig. 5 Typical real value of the complex signal H (*top*) and corresponding real value of its laplacian with a negative sign: $-\Delta H$ (*bottom*)

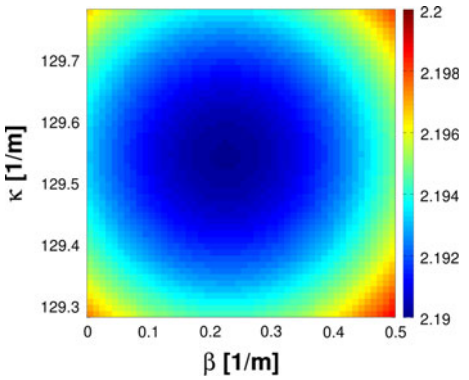

Fig. 6 Minimization of the norm $\left\|(\triangle + \mathbf{k}^2)H\right\|$ in the function of κ (the real part of the wavenumber **k**) and damping coefficient β (the imaginary part of the wavenumber **k**)

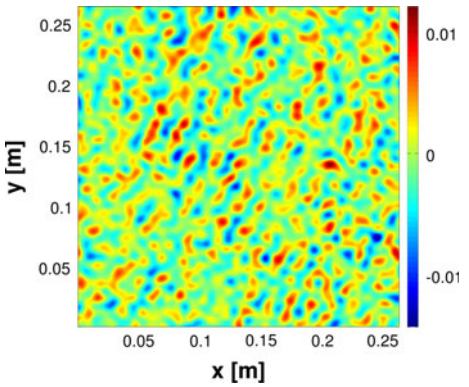

Fig. 7 Typical field of the minimization error $\varepsilon = (\triangle + \mathbf{k}^2_{\text{calc}})H$

measurements, it is possible to numerically compute the discrete laplacian

$$[\Delta H]_{ij} = \frac{1}{\Delta x^2}(H_{i-1,j} + H_{i+1,j} + H_{i,j-1} + H_{i,j+1} - 4H_{i,j}).$$

The field corresponding to $-\Delta H$ is shown in the Fig. 5 (bottom). Both patterns are very similar, indicating that the calculation of the wavenumber from the Helmholtz equation 3 can be achieved. To find the complex wavenumber **k,** we used the following method: from a given H pattern, the norm function $\left\|(\triangle + \mathbf{k}^2)H\right\|$ is minimized in the complex **k** plane. Figure 6 illustrates the minimization result. As it can be noticed from that plot, the minimum is found to be cylindrical and well defined.

The error of the minimization $\varepsilon = (\triangle + \mathbf{k}^2_{\text{calc}})H$ for the calculated wavenumber $\mathbf{k}_{\text{calc}}$ is shown in the Fig. 7. This error is one order of magnitude smaller than ΔH, and it is fairly randomly distributed in space.

3.2 Results

The above procedure allowed to determine the wavenumber **k** and thus the attenuation for surface waves on water

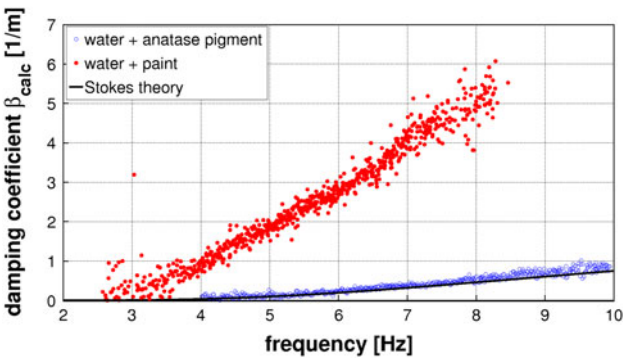

Fig. 8 Absolute damping coefficient β_{calc} in the function of the frequency. Comparison of the water suspensions obtained by adding anatase pigment and white paint. The *black line* is the theoretical attenuation β_0 given by Stokes (Eq. 5)

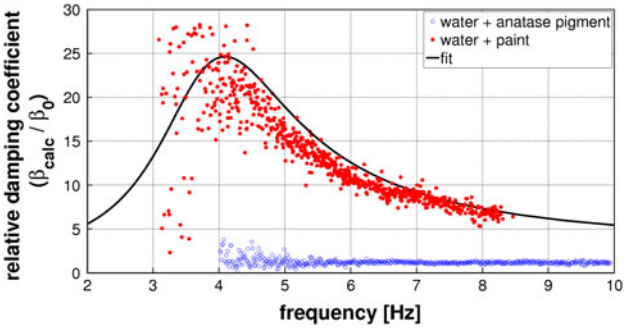

Fig. 9 Relative damping coefficient ($\beta_{\text{calc}}/\beta_0$) in the function of the frequency. Comparison of the water suspensions obtained by adding anatase pigment and white paint. The *black line* is the theoretical fit based on the formula proposed by Alpers (1989)

colored by titanium dioxide pigment (anatase) and colored by plain paint. The measured damping coefficient (β_{calc}) of these two different aqueous dispersions is compared in Fig. 8. The theoretical values for water with a clean surface are caused by the viscous attenuation in the bulk and are given by Stokes equation:

$$\beta_0 = \frac{4\kappa^2\mu\omega}{\rho g + 3\gamma\kappa^2} \tag{5}$$

We can notice that the attenuation of the titanium dispersion is comparable to the theoretical attenuation of the pure water, satisfying the aim of this study. The attenuation of the water colored by plain paint is many times larger than for the pure water and strongly depends on the frequency. It confirms that a viscoelastic film dramatically enhances the viscous energy dissipation in the boundary layer near the free surface.

Figure 9 shows the relative damping normalized by the damping of pure water. The theoretical prediction of the relative damping of water covered by a thin viscoelastic surface film is given by the Eq. 9 of Alpers (1989) (not reported here). It is compared to the measured attenuations

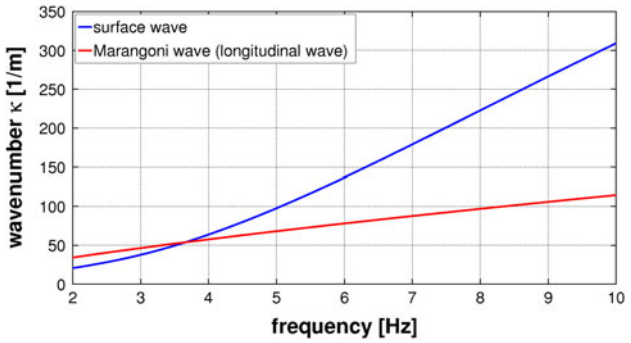

Fig. 10 Dispersion relation of the Marangoni and surface waves. The intersection region is the region of the dramatical increase in the wave energy dissipation

in the case of the water colored by plain paint, by fitting the surface-dilational modulus ε of the model. The black line in Fig. 9 shows the fit for which the absolute value of this modulus was found to be $|\varepsilon| = 0.033$ N/m and its phase angle $\theta = 180°$.

The maximum damping enhancement due to the surface film is found to be around 4 Hz where the attenuation with plain paint is 25 times larger than the attenuation of the water with clean surface. This damping resonance coincides with the intersection of the dispersion relation branches for the surface and Marangoni waves presented in the Fig. 10. The dispersion relation for Marangoni waves is given by:

$$\omega_M^3 = \left[\frac{-\mathrm{i}\varepsilon^2}{\rho\mu}\right]\mathbf{k}_M^4, \tag{6}$$

while for the water capillary-gravity waves, it is:

$$\omega_S^2 = g\mathbf{k}_S + \frac{\gamma}{\rho}\mathbf{k}_S^3 \tag{7}$$

Note also that based on the theoretical wave attenuation of the pure water (Eq. 5), the drop of the surface tension γ, caused by the presence of the surfactant, increases by itself the damping coefficient (without considering any resonance phenomena). Indeed, it was measured by Behroozi et al. (2007) that the decrease in the surface tension has influence on the attenuation jump.

Since the surface of suspension is exposed to ambient air, it becomes polluted as time evolves. Thus, the time range for which the suspension remains the damping equal to that of the pure water is in great interest for the experimentalists. Qualitative measurements were carried out systematically in time (for wave packet centered at 8 Hz). We observed a slow increase in the damping coefficient during the first 10 h. Further measurements revealed that a plateau is reached after 24 h. This enhancement of the attenuation cannot be neglected; however, it is small and does not exceed 35% of the original value. Practically, this pollution effect can be reduced by a careful surface aspiration which permits to restore the original value of the damping coefficient (where the original value means the value just after suspension preparation).

4 Conclusions

We have shown the great influence of the surface viscoelastic film on water wave attenuation when water is colored with plain paint for which the theoretical predictions of the Marangoni-surface wave resonance damping (studied by Alpers 1989) have been confirmed experimentally. Different types of titanium dioxide particles have been investigated in order to avoid the enhancement of damping. Eventually, the titanium dioxide anatase particles have been chosen to color water. They allow to perform space-time resolved FTP measurements of water waves with a damping equivalent to the clean surface case.

Acknowledgments We are thankful to Kronos for supplying us with Titanium dioxide particles. This work is founded by the ANR Tourbillonde and ProComedia.

Appendix

Let us consider the propagation of a plane wave in x positive direction (coordinate z being normal to the surface at rest) in an incompressible fluid with density ρ and dynamical viscosity μ. Neglecting the nonlinear terms, the Navier–Stokes equations for the velocity field $\mathbf{u} = [u_x, u_z]$ read:

$$\begin{aligned}\rho\frac{\partial u_x}{\partial t} &= -\frac{\partial p}{\partial x} + \mu\Delta u_x \\ \rho\frac{\partial u_z}{\partial t} &= -\frac{\partial p}{\partial z} + \rho g + \mu\Delta u_z\end{aligned} \tag{8}$$

where g denotes the gravity acceleration, and p is the pressure.

Considering the existence of the surface tension gradients, the kinematic boundary conditions on the surface (tangential and normal components, respectively) can be expressed as:

$$\begin{aligned}\frac{\partial\gamma}{\partial x} - \mathbf{T}_{xz} &= 0 \\ \gamma\frac{\partial^2\zeta}{\partial x^2} + p - p_a - \rho g\zeta - \mathbf{T}_{zz} &= 0\end{aligned} \tag{9}$$

where ζ denotes the surface elevation, p_a is the atmospheric pressure, and $\mathbf{T}$ the stress tensor. It has to be noted that the only difference in the whole mathematical formulation compared to the clean surface case is the nonzero tangential component of the stress tensor (due to the Marangoni effect of surface tension gradients). This gradient can be expressed as:

$$\frac{\partial \gamma}{\partial x} = \varepsilon \frac{\partial^2 \xi}{\partial x^2}$$

Here, ξ is the horizontal displacement of the surface, and ε denotes the surface-dilational modulus, which characterizes the viscoelastic fluid properties and is a complex number in general. The whole quantity is given by:

$$\varepsilon = |\varepsilon| \exp(-\mathrm{i}\theta)$$

A phase difference between the imposed area change and the surface tension variations, caused by a relaxation processes such as diffusion exchange, is expressed by the θ number.

Introducing the velocity field $\mathbf{u}$ as a sum of the velocity potential Φ (providing an irrotational field) and the vorticity function Ψ (providing a divergence-free field) and assuming zero velocity at infinite depth, we can obtain the harmonic wave solutions to the linearized Navier–Stokes equations (8).

Substituting these solutions into boundary conditions (9), it can be shown that the system has two solutions at each frequency. One solution corresponds to the classical capillary-gravity water wave and the other to the Marangoni wave. Lucassen (1968) showed experimentally that the wavelength of the capillary-gravity wave does not depend on the surface viscoelastic properties (is almost independent of ε), while the imaginary part of their wavenumber (damping coefficient) is strongly dependent on ε.

A simple way to obtain the dispersion relation of the Marangoni wave is to take the tangential component of the force balance at the surface assuming a horizontal Stokes boundary layer in the fluid:

$$\varepsilon \frac{\partial^2 \xi}{\partial x^2} \simeq \mu \frac{\partial u_x}{\partial z}$$

Then, the derivative $\partial_z u_x$ is equal to $m u_x$ (with the exponential decrement of the Stokes boundary layer $m = \sqrt{\mathrm{i}\omega\rho/\mu}$). Eventually, the continuity of horizontal velocity between the film surface and the fluid, $u_x = i\omega\xi$, is used to obtain

$$\varepsilon \frac{\partial^2 \xi}{\partial x^2} = i\mu\omega m \xi$$

that yields the dispersion relation for the Marangoni wave, given by Eq. 6.

This Marangoni wave is strongly damped. Assuming purely elastic film (ε is a real quantity) and denoting $\mathbf{k}_M = \kappa_M + \mathrm{i}\beta_M$:

$$\begin{aligned} \kappa_M &= \cos(\pi/8)\left(\frac{\rho\mu}{\varepsilon^2}\right)^{1/4} \omega_M^{3/4} \\ \beta_M &= \tan(\pi/8)\kappa_M \approx 0.414\kappa_M \end{aligned} \tag{10}$$

The real and imaginary part are of the same order of magnitude—the longitudinal waves are damped out very rapidly!

The capillary-gravity waves and surface waves are in general not oscillating with the same frequency and wavelength. However, the character of the dispersion relations allows to intersect the frequency-wavelength branches (Fig. 10). When the frequencies and wavelengths of the capillary-gravity wave and Marangoni wave are equal, the particle motion coincides for both waves, giving rise to a high velocity gradients in a Stokes boundary layer just beneath the surface film. This explains why the strongest enhancement of damping of capillary-gravity wave is found to be around the transverse-longitudinal resonance values.

References

Alpers W, Hühnerfuss H (1989) The damping of ocean waves by surface films: a new look at an old problem. J Geophys Res 94(5):6251–6265

Behroozi P, Cordray K, Griffin W, Behroozi F (2007) The calming effect of oil on water. Am J Phys 75:407–414

Cini R, Lombardini PP, Manfredi C, Cini E (1987) Ripple damping due to monomolecular films. J. Colloid Interface Sci 119:74–80

Cobelli P, Pagneux V, Maurel A, Petitjeans P (2009) Experimental observation of trapped modes in a water wave channel. Euro Phys Lett 88:20006

Cobelli P, Maurel A, Pagneux V, Petitjeans P (2009) Global measurement of water waves by Fourier transform profilometry. Exp Fluids 46:1037–1047

Cobelli P, Pagneux V, Maurel A, Petitjeans P (2011a) Experimental study on water-wave trapped modes. J Fluid Mech 666:445–476

Cobelli P, Przadka A, Petitjeans P, Lagubeau G, Pagneux V, Maurel A (2011b) Different regimes for water wave turbulence. Phys Rev Lett 107:214503

Ermakov SA, Zujkova AM, Panchenko AR, Salashin SG, Talipova TG, Titov VI (1986) Surface film effect on short wind waves. Dyn Atmos Oceans 10:31–50

Evans DF, Wennerström H (1994) The colloidal domain. VCH, Wiley, New York

Franklin B (1774) Of the stilling of waves by means of oil. Philos Trans 64:445–460

Gorthi SS, Rastogi P (2010) Fringe projection techniques: whither we are? Opt Lasers Eng 48(2):133–140

Hunter R (1981) Zeta potential in colloid science. Academic Press, New York

Israelachvili J (1991) Intermolecular and surface forces. Academic Press, New York

Lagubeau G, Fontelos M, Josserand C, Maurel A, Pagneux V, Petitjeans P (2010) Rosace patterns in drop impact. Phys Rev Lett 105:184503

Lange P, Hühnerfuss H (1984) Horizontal surface tension gradients induced in monolayers by gravity wave action. J Phys Oceanogr 14:1620–1628

Levich VG (1962) Physicochemical hydrodynamics. Prentice-Hall, Elmsford Park

Lucassen J (1968) Longitudinal capillary waves. Part 1—theory. Trans Faraday Soc 64:2221–2229

Lucassen J (1982) Effect of surface-active material on the damping of gravity waves: a reappraisal. J Colloid Interface Sci 85:52–58

Marangoni C (1872) Sul principio della viscosita superficiale dei liquidi stabili. Nuovo Cimento Ser 5/6(2):239–276

Maurel A, Cobelli P, Pagneux V, Petitjeans P (2009) Experimental and theoretical inspection of the phase-to-height relation in Fourier transform profilometry. Appl Opt 48(2):380–392

Miles JW (1967) Surface wave damping in closed basins. Proc R Soc Lond A 297:459–475

Prisle NL, Raatikainen TR, Sorjamaa R, Svenningsson B, Laaksonen A, Bilde M (2008) Surfactant partitioning in cloud droplet activation: a study of C8, C10, C12 and C14 normal fatty acid sodium salts. Tellus B 60:416–431

Takeda M, Mutoh K (1983) Fourier transform profilometry for the automatic measurement of 3-D object shapes. Appl Opt 22:3977–3982

Takeda M, Ina H, Kobayashi S (1982) Fourier-transform method of fringe-pattern analysis for computer-based topography and interferometry. J Opt Soc Am 72(1):156–160